Better symplectic integration of rigid body rotation

Toshio Fukushima
National Astronomical Observatory of Japan,
2-21-1, Ohsawa, Mitaka, Tokyo 181-8588, Japan
Toshio.Fukushima@nao.ac.jp

Abstract

The accumulation of the round-off errors causes the linear drift of the conserved quantities of the rigid body rotation simulated by the existing symplectic integrators. This associates with the quadratic deviation in the orientation of the rotating body. The phenomenon is eminent in the single precision integration and in the long-term double precision integration. We suppress it by rewriting the two-dimensional rotation operation used in the integrators into a leap-frog form. The resulting new symplectic integrators realize a meaningful single precision simulation of the rigid body rotation.

1 Introduction

1.1 Symplectic integration of the rigid body rotation

The symplectic integration is a popular tool to study various dynamical systems numerically (Sanz-Serna, 1992; Sanz-Sema and Calvo, 1994; Hairer et al., 2002; Leimkuhler and Reich, 2004). The rotational motion of rigid bodies is no exception (Ge and Marsden, 1988). It is vitally investigated in the molecular dynamics and astrophysics (Bond et al., 1999; Marsden et al., 1999; Benettin et al., 2001; Miller et al., 2002; Hairer, 2003; McLachlan and Zanna, 2004; Hairer and Vilmart, 2006; Okumura et al., 2007; Ortolan and Saccon, 2012). Refer to Fassò (2003) comparing three major symplectic integrators of the rigid body rotation (McLachlan, 1993; Reich, 1994; Touma and Wisdom, 1994).

Recently, some integrators were proposed to utilize the analytical solution of the torque-free rotation of an asymmetric rigid body (Celledoni and Säfström, 2006; van Zon and Schofield, 2007a,b; Celledoni et al., 2007). This is at the cost of a significant increase in CPU time at each time step since it requires the numerical evaluation of some special functions: the Jacobian

elliptic functions and the incomplete elliptic integral of the third kind regarded as a function of that of the first kind (Fukushima, 2009c). As for the precise and fast computation of these elliptic functions and elliptic integrals, refer to a series of our works (Fukushima, 2009a,b, 2010, 2011a,b,c, 2012). When the torque is sufficiently small as in the case of asteroids in the solar system (Fukushima, 2008a,b,c), this formulation enables us choosing a large step size, and therefore, the total computational time is expected to decrease significantly.

1.2 Problem of the existing symplectic integration

Vilmart (2008) discovered that the symplectic integrators using the analytical solution of the torque-free rotation have a problem: an undesired linear growth of the energy error. He conjectured that this is caused by uneven appearance of local round-off errors in evaluating the body-fixed components of the angular velocity vector by the elliptic functions. Since this phenomenon appears even in the torque-free rotation, it becomes a serious trouble in all the rotational motions.

We conducted a similar investigation on the symplectic integration of the rigid body rotation by the integrators without using the elliptic functions and integrals. Fig. 1 shows the averaged energy errors of the torque-free rotation of a single water molecule integrated by the 3R splitting method (Dullweber et al., 1997) in the single precision environment. We omit the results obtained by the other symplectic integrators, i.e. those of the type SR or RS in terms of Fassò (2003). This is because all of them give essentially the same results and the 3R approach is the best for a water molecule (Dullweber et al., 1997).

Plotted are the relative errors of the rotational energy as a function of time. The marks in Fig. 1 illustrate the mean values of 1000 integrations with different initial conditions. The initial values of the body-fixed components of the angular velocity vector were randomly chosen while the magnitude of the vector is kept the same. Meanwhile, the initial values of the orientation matrix were produced from the Euler parameters the numerical values of which were randomly assigned while satisfying the unitary condition. The standard deviations of the energy errors with respect to the initial values are shown as the error bars although they are hardly visible at this scale.

The observed energy dissipation mostly disappears in the double precision integration as will be seen later in §3.3. Also, the smaller the step size is,

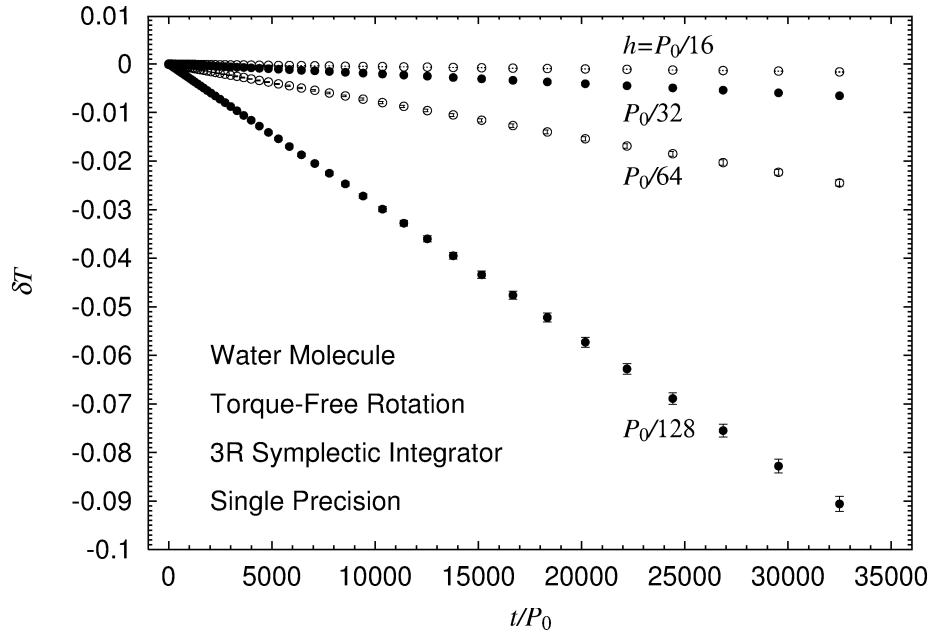

Figure 1: Linear decrease of the rotational energy of the torque-free rotation of a water molecule obtained by the existing symplectic integrator. The averaged relative errors of the rotational energy, $\delta T \equiv (T - T_0)/T_0$, for some different step sizes are plotted as a function of the physical time, t. Here $P_0 \equiv 2\pi/\omega_0$ is the initial period of rotation.

the larger the energy error becomes. This is in the opposite sense to the results of the non-symplectic integrators such as the fourth-order Runge-Kutta method. These facts indicate that the observed phenomenon is induced by the accumulation of round-off errors. Dullweber et al. (1997) already noted this kind of feature in explaining their Figs 13 and 14.

An artificial energy dissipation occurs independently on the initial conditions. This fact is troublesome and hinders us to extract the physically meaningful conclusions from the results of single precision simulation even though they seem to be stationary and/or ordered.

1.3 Solution to the problem

Traditionally, the problem of accumulation of the round-off errors in the numerical integration has been studied mainly for the multistep methods to integrate the astronomical orbital motions (Brouwer, 1937; Henrici, 1962; Quinlan, 1994; Fukushima, 1996; Grazier et al., 2004/05). Recently, it is also discussed for the symplectic integration in particle physics and astrophysics (Karney, 1986; Scovel, 1991; Earn and Tremaine, 1992; Petit, 1998; Skeel, 1999; Fukushima, 2001; Hairer et al., 2008; Vilmart, 2008). Among various devices proposed, we applied the idea of Karney (1986) to the present case. Then, we succeeded to resolve this undesired situation in the rotational motion by a slight modification of the existing symplectic integrators: the rewriting of the two-dimensional rotation operation into a leap-frog form.

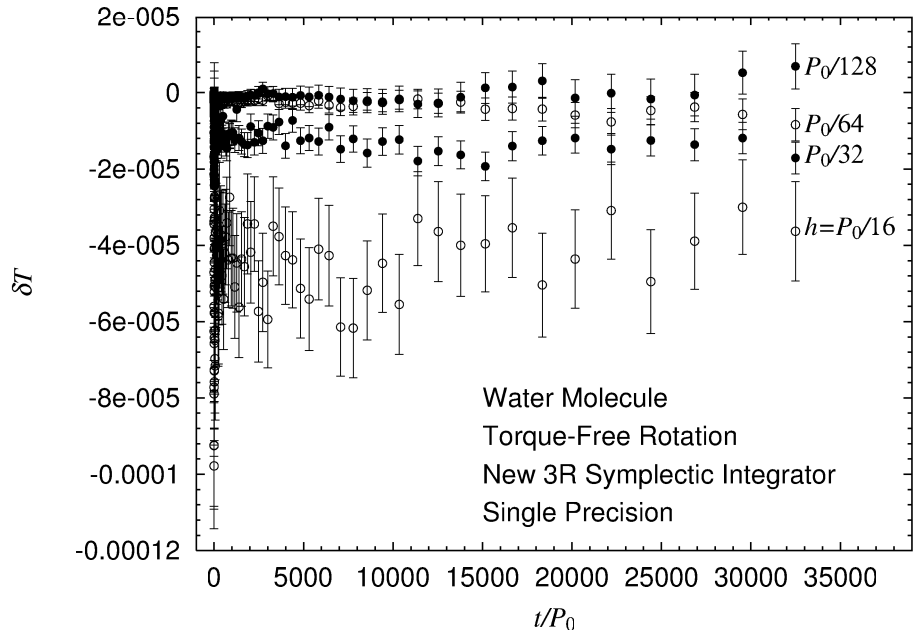

Figure 2: Constancy of the rotational energy of the torque-free rotation of a water molecule obtained by the new symplectic integrator. Same as Fig. 1 but after the rewriting of the two-dimensional rotation operation into a leap-frog form.

Fig. 2 illustrates that the rewritten integrator keeps the constancy of the

rotational energy as we anticipate for the ideal symplectic integrators. This time, the averaged deviation diminishes according as the step size decreases. This indicates that the deviations are mainly caused by the truncation errors. In this short article, we explain this new technique and present some illustrations of its performance.

2 Method

2.1 Two-dimensional rotation

Many symplectic integrators of the rigid body rotation use the two-dimensional rotation operation as a building block (Fassò, 2003):

$$\begin{pmatrix} x_{n+1} \\ y_{n+1} \end{pmatrix} = \begin{pmatrix} \cos\theta & -\sin\theta \\ \sin\theta & \cos\theta \end{pmatrix} \begin{pmatrix} x_n \\ y_n \end{pmatrix}, \tag{1}$$

where x and y are either (1) two among three body-fixed components of the rotational angular momentum, (2) two among three unit vectors consisting of the orientation matrix, or (3) two among four components of the Euler parameters (or the unit quaternion) (McLachlan, 1993; Reich, 1994; Touma and Wisdom, 1994; Dullweber et al., 1997).

For example, the 3R splitting method of the ordering 1-2-3-2-1 uses the product of five rotations,

$$R_1\left(\frac{h\omega_A^{(n+1)}}{2}\right) \circ R_2\left(\frac{h\omega_B^{(n+1)}}{2}\right) \circ R_3\left(h\omega_C^{(n+1/2)}\right) \circ R_2\left(\frac{h\omega_B^{(n)}}{2}\right) \circ R_1\left(\frac{h\omega_A^{(n)}}{2}\right), \tag{2}$$

where (1) $R_j(\theta)$ denotes the two-dimensional rotation operation around the j-th axis by the rotation angle θ, (2) h is the step size of the integration, (3) $\omega_A\,(=\omega_1)$, $\omega_B\,(=\omega_2)$, and $\omega_C\,(=\omega_3)$, are the three body-fixed components of the angular velocity vector, and (4) the superscript denotes the index of timing such that (n) means when $t = t_n \equiv t_0 + nh$.

2.2 Rewriting

By increasing the precision of each component of the existing symplectic integrator part by part, we find that the two-dimensional rotation operation is the source of serious accumulation of the round-off errors we observed in

Fig. 1. In order to suppress the local production of the round-off errors, we follow the idea of Karney (1986) to rewrite the two-dimensional rotation matrix into a triple product of shear matrices as

$$\begin{pmatrix} x_{n+1} \\ y_{n+1} \end{pmatrix} = \begin{pmatrix} 1 & 0 \\ \tau & 1 \end{pmatrix} \begin{pmatrix} 1 & -\sigma \\ 0 & 1 \end{pmatrix} \begin{pmatrix} 1 & 0 \\ \tau & 1 \end{pmatrix} \begin{pmatrix} x_n \\ y_n \end{pmatrix}, \tag{3}$$

where

$$\tau \equiv \tan\frac{\theta}{2}, \quad \sigma \equiv \sin\theta = \frac{2\tau}{1+\tau^2}. \tag{4}$$

If the rotation matrix is approximated, as usually done in the molecular dynamics simulation (Dullweber et al., 1997, Appendix A), as

$$\cos\theta \approx \frac{4-\theta^2}{4+\theta^2}, \quad \sin\theta \approx \frac{4\theta}{4+\theta^2}, \tag{5}$$

we achieve the same approximation by setting τ as

$$\tau \approx \frac{\theta}{2}. \tag{6}$$

In general, we may adopt the higher order approximations by truncating the Maclaurin series expansion of the tangent function as

$$\tau = \frac{\theta}{2} + \frac{\theta^3}{24} + \frac{\theta^5}{240} + \frac{17\theta^7}{40320} + \frac{31\theta^9}{725760} + \cdots. \tag{7}$$

For example, the first four terms are enough to construct an eighth-order integrator by the composition method (Hairer et al., 2002, Section II.4).

2.3 Interpretation as the leap-frog integration

Introducing an intermediary variable, $y_{n+1/2}$, we interpret the rewritten operation as the leap-frog integration of a one-dimensional harmonic oscillator as

$$\begin{cases} y_{n+1/2} = y_n + \tau x_n, \\ x_{n+1} = x_n - \sigma y_{n+1/2}, \\ y_{n+1} = y_{n+1/2} + \tau x_{n+1}, \end{cases} \tag{8}$$

where x and y are understood as the velocity and the coordinate of the oscillator, τ plays a role of the step size, and $\sigma/\tau = 2/(1+\tau^2)$ is regarded as the square of the angular velocity of the oscillation. An actual computing code becomes much simpler:

```
y += x * tau;
x -= y * sigma;
y += x * tau;
```

Obviously, this procedure is time-reversible. We anticipate that the successive application of this leap-frog form leads to a better behavior in the local production of the round-off errors and their global accumulation. Indeed, we experimentally learn that this form ensures the random feature of round-off errors.

2.4 Errors of the rewritten operation

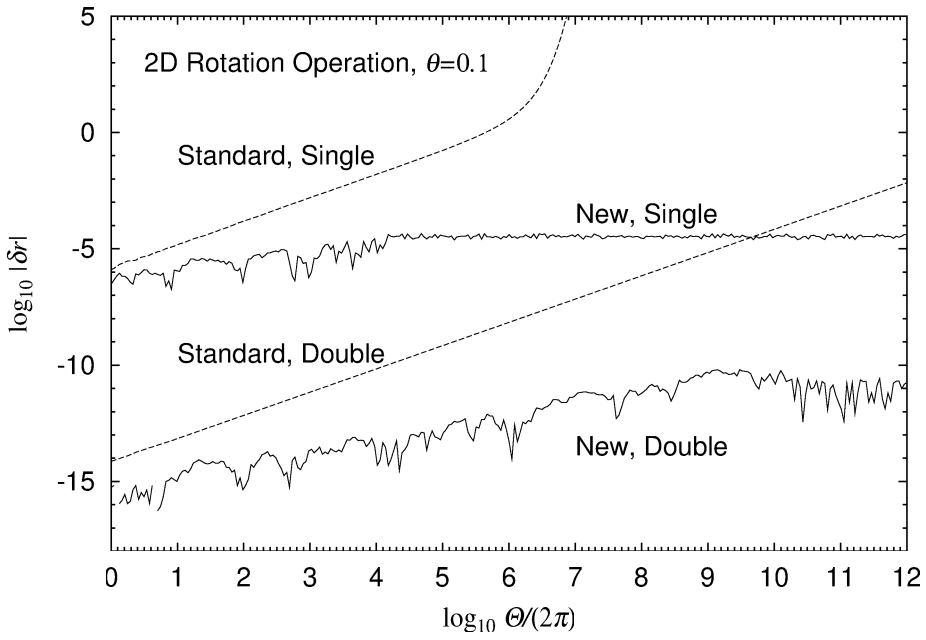

Figure 3: Error growth of the accumulated two-dimensional rotation operation. The incremental rotation angle, θ, is fixed as 0.1 radian.

Fig. 3 compares the relative errors of the norm of the rotated unit vector, $\delta r_n \equiv \left(\sqrt{x_n^2 + y_n^2}/\sqrt{x_0^2 + y_0^2}\right) - 1$, obtained by the standard and the new operations in the single and the double precision environments, respectively. We set the initial values as $x_0 = 1.0$ and $y_0 = 0.0$ and the incremental

rotation angle as $\theta = 0.1$. Since $\theta/(2\pi)$ is irrational, the integrated rotation state will be ergodic.

In conducting the numerical experiments, all the computation codes were (1) written in Fortran 90, (2) compiled by the Intel Visual Fortran Composer XE 2011 update 8 with the level 3 optimization, and (3) executed at a PC with an Intel Core i7-2675QM CPU and 16 GB main memory run at the clock 2.20 GHz under the 64 bit Windows 7 OS.

The errors are plotted as functions of the accumulated rotation angle, $\Theta \equiv n\theta$, in a log-log manner. In the case of the standard implementation of the rotational operation, the errors increase linearly. Once exceeding unity, they grow exponentially. This feature is irrelevant with the computing precision.

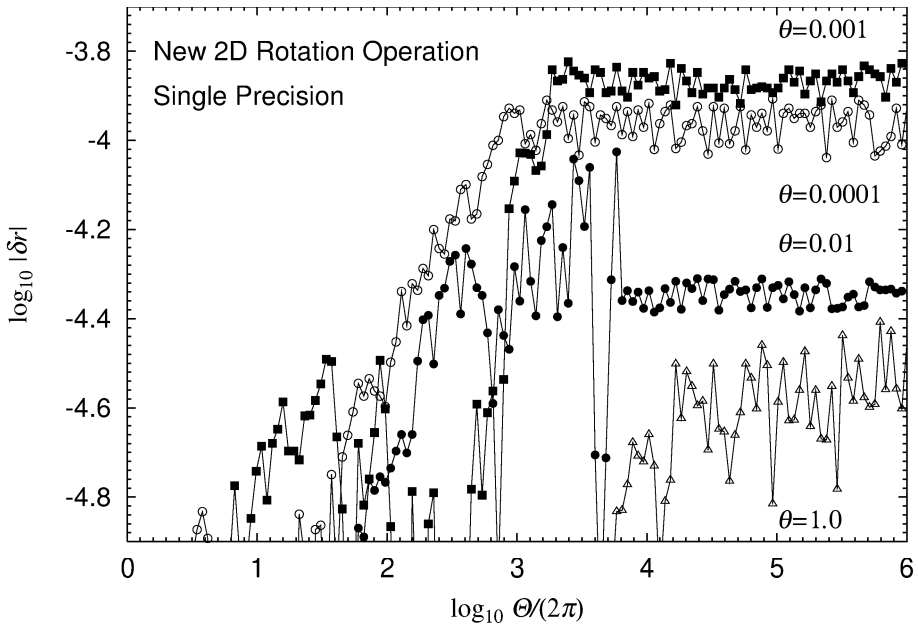

Figure 4: Stationary phenomena of the error growth of the new two-dimensional rotation operation. Same as the curve of the new method in the single precision computation in Fig. 3 but for different values of θ. The stationary value of $|\delta r|$ for the case $\theta = 0.1$, which was already shown in Fig. 3, is between those for $\theta = 1.0$ and $\theta = 0.01$.

On the other hand, in the case of the new method, the errors are oscillating and their magnitude increases in proportion to the square root of

time initially. This means that the local production of the round-off errors are stochastic and there are no correlation among the local errors (Henrici, 1962). It is the best feature expected in the long-term numerical integration of the action variables (Brouwer, 1937).

However, the expectation is betrayed in a good sense. The magnitude of the errors of the new method seems to be stationary when it reaches a certain amount. Refer to Fig. 3 again. In this specific case, the stationary values are around 3×10^{-5} and 2×10^{-11} in the single and the double precision environments, respectively. This is quite interesting.

Fig. 4 shows this stationary phenomenon for a wide variety of the incremental rotation angle θ, say ranging from 10^{-4} to 1.0 radian. We have no theoretical explanation about this behavior. There is no resonant feature since the ratios of the tested incremental rotation angles to the period, 2π, are irrational.

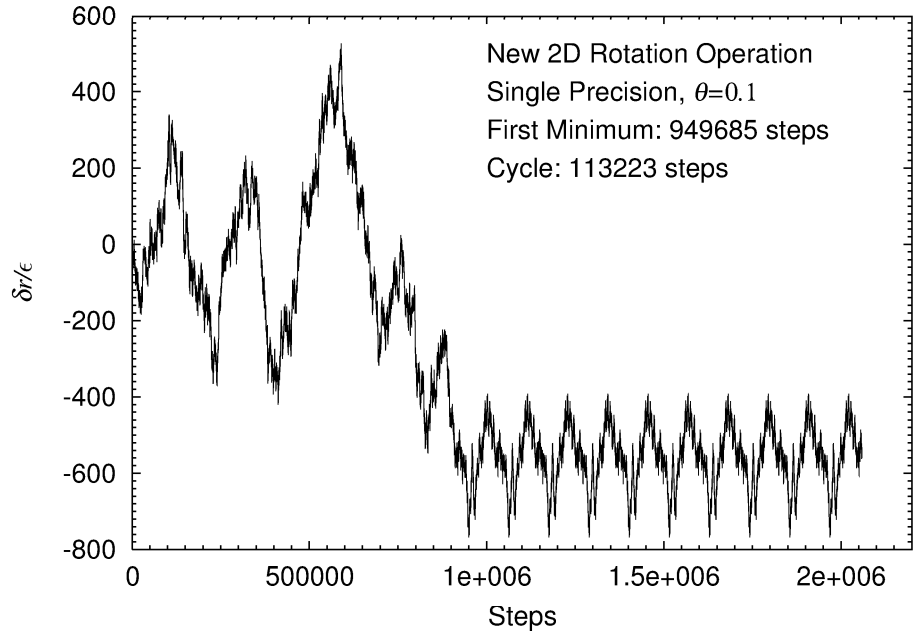

Figure 5: Limit cycle of the new two-dimensional rotation operation.

We find that this is caused by a fact that the mapping of the new two-dimensional rotation operation is trapped into a limit cycle. Refer to Fig. 5. This is similar to the situation observed in Fig. 1 of Skeel (1999), where an

exactly periodic mapping is achieved in a sort of lattice phase space. Curious is the fact that we take no special care for rounding in the present case. At any rate, Fig. 3 shows the benefit of rewriting into a leap-frog form.

3 Numerical experiments

Let us examine the computational cost and performance of the new method. As we observed in the previous section, the implementation of the new method is simple. Also, the rewritten computational code becomes a little more compact, and therefore, it runs slightly faster than before rewriting. Nevertheless, the comparison of the computational speed in the part of the torque-free rotation is less meaningful. In practical cases, the torque computation occupies more than 99% of the total CPU time. Thus, we concentrate ourselves to the question of the computing precision.

3.1 Torque-free rotation

Figs 1 and 2 already depicted the manner of error growth of the rotational energy, T, obtained by the existing and the new symplectic integrators of the rigid body rotation in the single precision environment. Here, T is defined as

$$T \equiv \frac{1}{2}\left(A\omega_A^2 + B\omega_B^2 + C\omega_C^2\right), \tag{9}$$

where $A\,(= I_1)$, $B\,(= I_2)$, and $C\,(= I_3)$ are the principal moments of inertia of the rotating body in the order of magnitude, $A \leq B \leq C$. In the case of a water molecule, their ratios are significantly smaller than unity as $A/C = 0.345$ and $B/C = 0.653$, respectively.

Let us examine the errors of the other conserved quantities. One is a norm of the orientation matrix defined as

$$R \equiv \sqrt{\left(\vec{e}_A\right)^2 + \left(\vec{e}_B\right)^2 + \left(\vec{e}_C\right)^2}, \tag{10}$$

where $\vec{e}_A$ denotes the unit vector in the direction of the A-axis, and so on. This is a mathematical constant, and therefore, must be the same independently on (1) the initial conditions, (2) the ratios of the principal moments of inertia, or (3) the magnitude and the nature of the considered torque.

Another conserved quantities are the inertial components of the rotational angular momentum vector defined as

$$S_X \equiv \vec{S} \cdot \vec{e}_X, \quad S_Y \equiv \vec{S} \cdot \vec{e}_Y, \quad S_Z \equiv \vec{S} \cdot \vec{e}_Z, \tag{11}$$

where $\vec{e}_X$ is the unit vector toward the direction of the X-axis, and so on, and

$$\vec{S} \equiv A\omega_A \vec{e}_A + B\omega_B \vec{e}_B + C\omega_C \vec{e}_C, \tag{12}$$

is the rotational angular momentum vector.

Figs 6 and 7 show the time dependence of the relative errors of these conserved quantities of the torque-free rotation. They are the results of the single precision integration with the step size, $h = P_0/32$, by the 3R symplectic integrator and its rewriting, respectively. Here, we plotted the results averaged with respect to 1000 random initial conditions. Obviously, the errors of the existing symplectic integrator contain linear drifts in all the conserved quantities while those of the new method are all constant.

3.2 Rotation under an autonomous torque

Let us move to the rotation under a torque. The torque vector is expressed in the body-fixed frame as

$$\vec{N} = N_A \vec{e}_A + N_B \vec{e}_B + N_C \vec{e}_C, \tag{13}$$

where N_A through N_C are the body-fixed components of the torque vector.

As an example of the autonomous torque, we consider the torque caused by a constant attraction toward the negative z-axis. In this case, N_A through N_C are written as

$$N_A = 3\lambda\alpha n_C n_B, \quad N_B = 3\lambda\beta n_A n_C, \quad N_C = 3\lambda\gamma n_B n_A, \tag{14}$$

where α, β, and γ are the inertia parameters expressed as

$$\alpha \equiv \frac{C-B}{A}, \quad \beta \equiv \frac{A-C}{B}, \quad \gamma \equiv \frac{B-A}{C}, \tag{15}$$

while n_A through n_C are the cosines to the attraction direction written as

$$n_A \equiv \vec{e}_A \cdot \vec{e}_Z, \quad n_B \equiv \vec{e}_B \cdot \vec{e}_Z, \quad n_C \equiv \vec{e}_C \cdot \vec{e}_Z, \tag{16}$$

and λ is a parameter characterizing the relative strength of the torque.

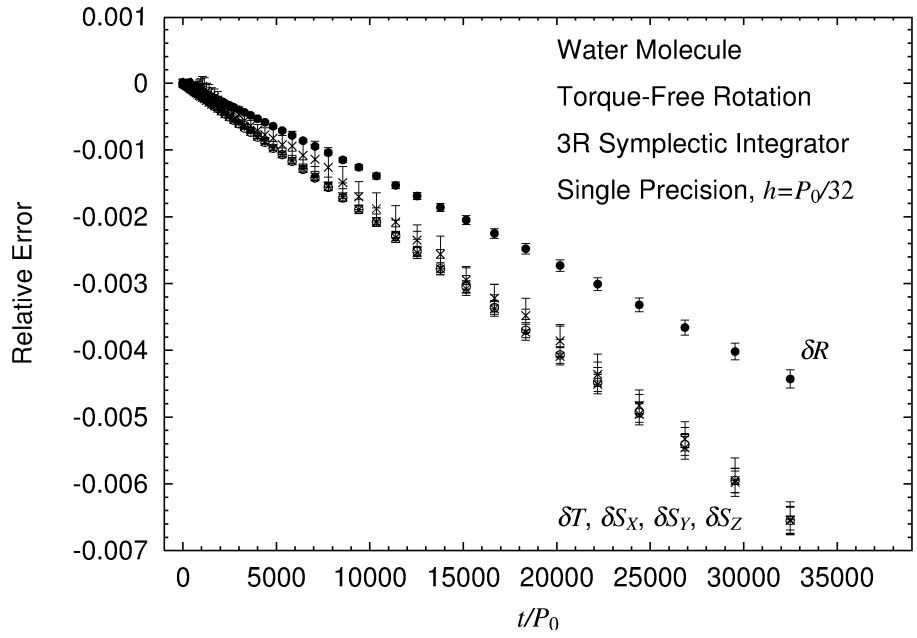

Figure 6: Linear drift of the five conserved quantities of the torque-free rotation of a water molecule obtained by the existing symplectic integrator. Same as Fig. 1 but for T, R, S_X, S_Y, and S_Z when $h = P_0/32$.

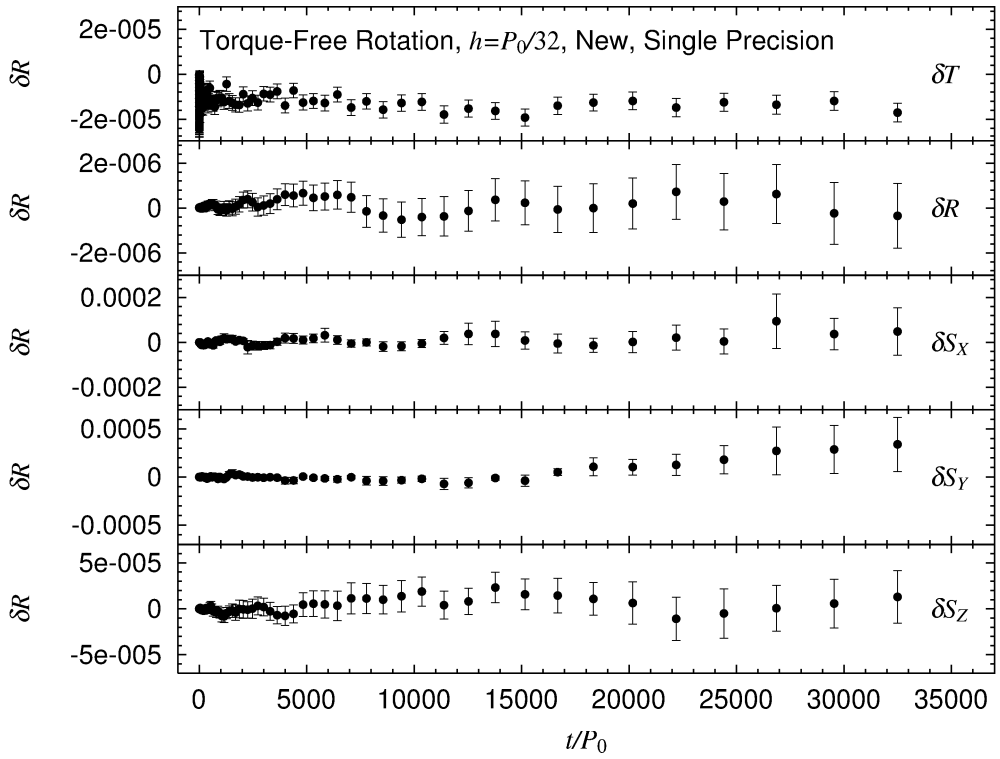

Figure 7: Constancy of the five conserved quantities of the torque-free rotation of a water molecule obtained by the new symplectic integrator. Same as Fig. 6 but obtained by the new integrator.

In this case, the conserved quantities are R, S_Z, and the total energy, E, defined as

$$E \equiv T + U, \tag{17}$$

where the potential energy U is written as

$$U \equiv -\left(\frac{3\lambda}{4}\right)\left[(A+B-2C)n_C^2 + (B-C)\left(n_A^2 - n_B^2\right)\right]. \tag{18}$$

Fig. 8 plots the relative errors of the total energy of the rotation simulated by the 3R symplectic integrator where we set $\lambda = 1$. This value of λ corresponds to the case of a fairly strong torque. Again, we illustrated the statistical results of a water molecule with 1000 different initial conditions randomly chosen. Although the standard deviations become somewhat larger, the observed linear drifts remain unchanged. On the other hand, Fig. 9 shows the time dependence of the three conserved quantities, E, R, and S_Z, of the rotations computed by the new symplectic integrator. All of them are mostly constant with time.

3.3 Double precision integration

If we conduct the symplectic integration in the double precision environment, the feature of the existing method observed in the previous subsections almost disappears. Refer to Fig. 10 for the constancy of four among five conserved quantities of the torque-free rotation of a water molecule when $h = P_0/32$. Again, we plotted the averaged results starting from 1000 different initial conditions chosen randomly.

An exception is the norm of the orientation matrix, R, as shown in Fig. 11. There remains a tiny but secular drift in its errors. We observed essentially the same feature when an autonomous torque is acted on the rotating body.

On the other hand, the constancy of all the conserved quantities is maintained by the new integrator. Refer to Fig. 12. The magnitude of the periodic component of δT is unchanged in the double precision integration. Meanwhile, the magnitude of the averaged deviations of the other quantities drastically reduced in the double precision computation.

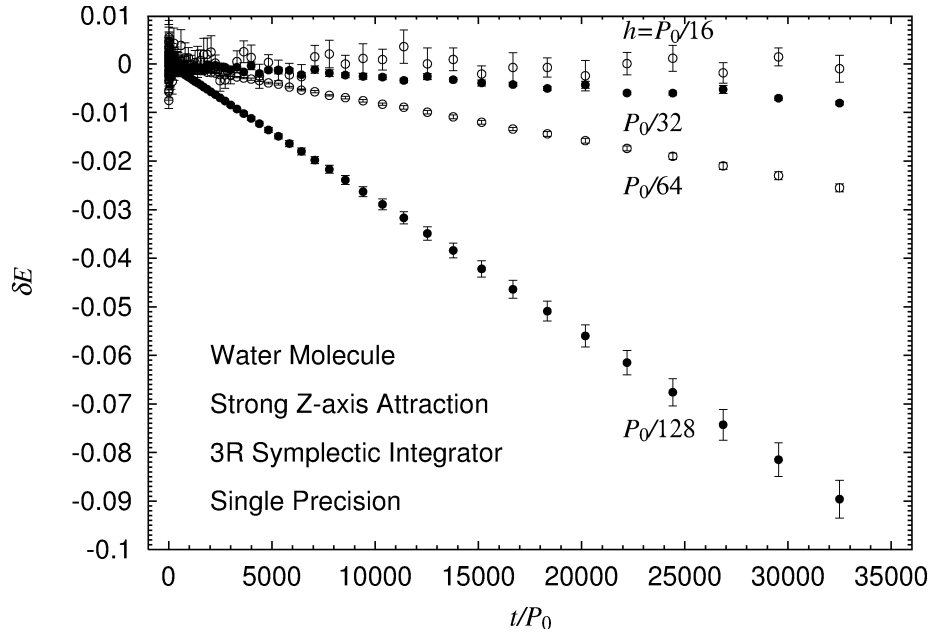

Figure 8: Linear drift of the total energy of rotation of a water molecule under a strong torque obtained by the existing symplectic integrator. Same as Fig. 1 but for the total energy, E, of the rotation of a water molecule pulled by a strong attraction toward the negative z-direction.

Table 1: Nontrivial composition coefficients of a fourth order integrators

	Omelyan et al. (2002, Eq.(35))
p	4
s	5
d_1	+0.3221375960817984
d_2	+0.5413165481700430

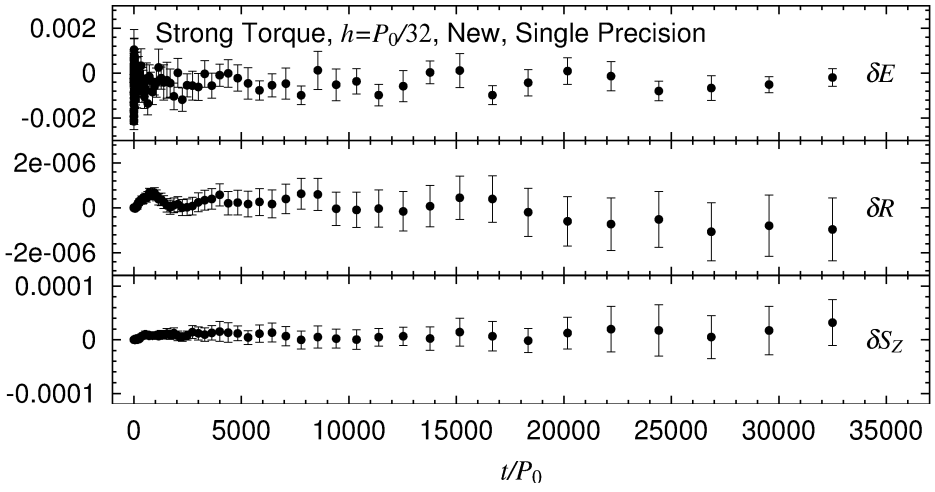

Figure 9: Constancy of three conserved quantities of the rotation of a water molecule under a strong torque obtained by the new symplectic integrator. Same as Fig. 7 but for the rotation under the torque caused by a strong z-direction attraction when $h = P_0/32$.

Table 2: Nontrivial composition coefficients of a sixth order integrators

	Kahan and Li (1997, `s9odr6a`)
p	6
s	9
d_1	+0.3921614440073141
d_2	+0.3325991367893594
d_3	−0.7062461725576393
d_4	+0.0822135962935508

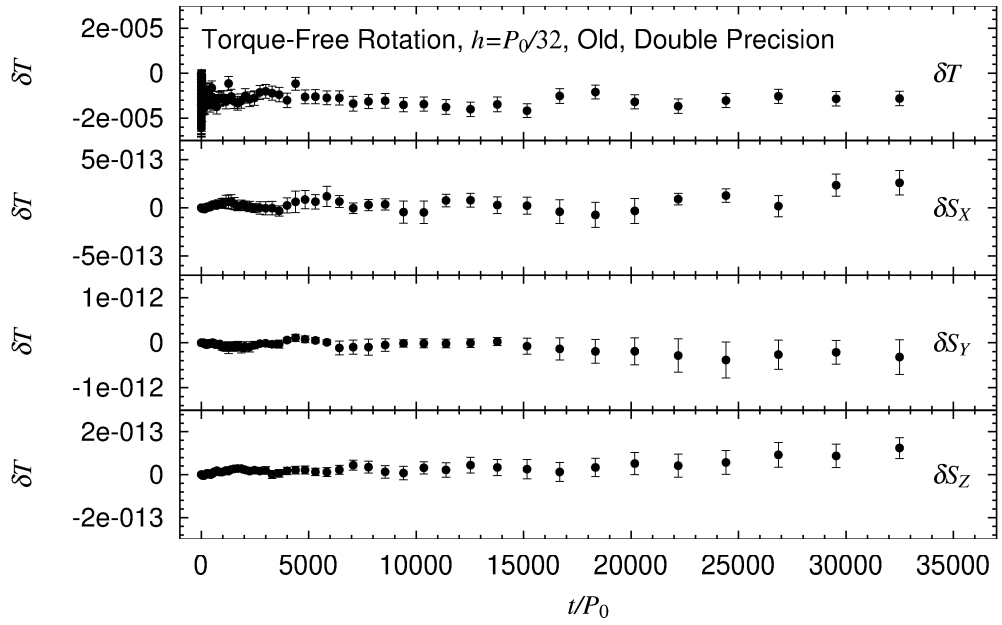

Figure 10: Constancy of the four conserved quantities of the torque-free rotation of a water molecule. Same as Fig. 7 but for T, S_X, S_Y, and S_Z obtained by the existing symplectic integrator in the double precision environment.

Table 3: Nontrivial composition coefficients of an eighth order integrators

Kahan and Li (1997, `s17odr8a`)	
p	8
s	17
d_1	+0.1302024830888900
d_2	+0.5611629817751083
d_3	−0.3894749626448472
d_4	+0.1588419065551556
d_5	−0.3959038941332375
d_6	+0.1845394609783157
d_7	+0.2583743876863220
d_8	+0.2950117236093102

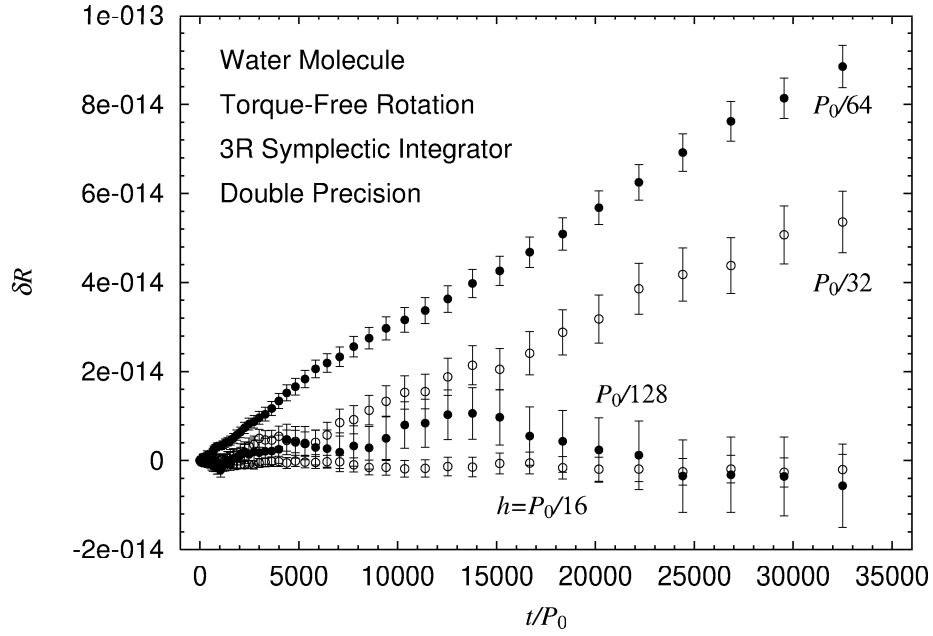

Figure 11: Secular drift of the norm of the orientation matrix of the torque-free rotation of a water molecule obtained by the existing symplectic integrator. Same as Fig. 10 but for the norm of the orientation matrix, R.

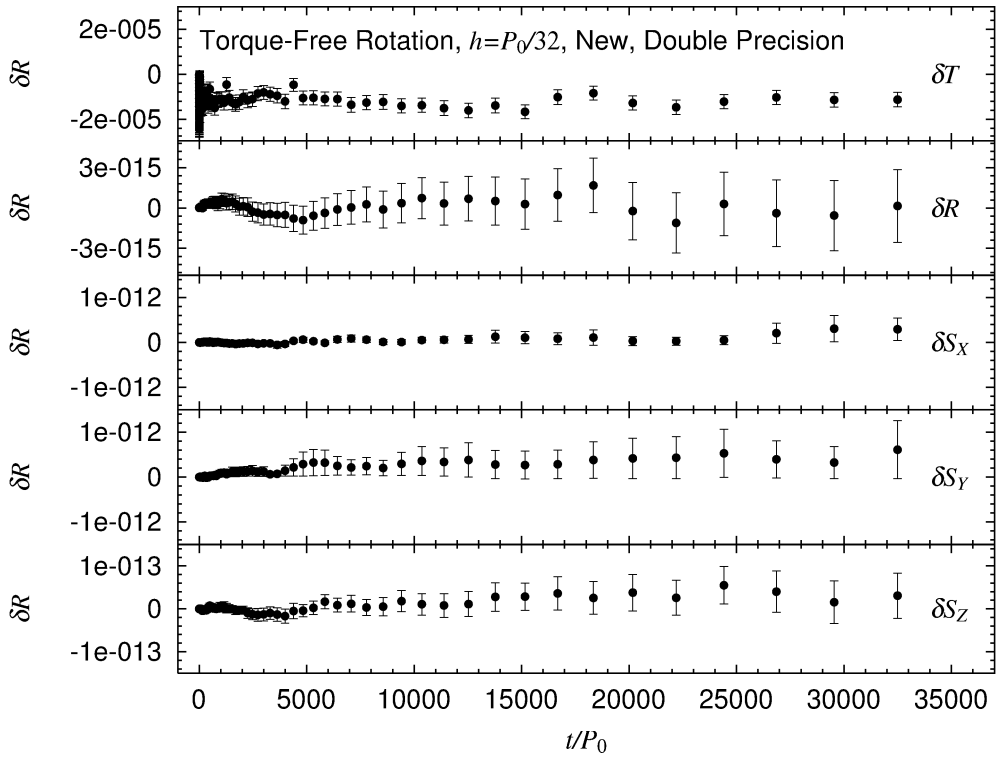

Figure 12: Constancy of the five conserved quantities of the torque-free rotation of a water molecule obtained by the new symplectic integrator in the double precision environment.

3.4 High order integration

Let us examine whether the observed behavior of the second-order symplectic integrators is common to the case of higher order integrators. We construct the fourth-, the sixth-, and the eighth-order methods from the corresponding second-order ones by the composition method (Hairer et al., 2002, Section II.4). A p-th order, s-stage integrator is time-symmetrically composed as

$$S_p(h) \equiv S_2(d_1 h) \circ \cdots \circ S_2(d_{s-1} h) \circ S_2(d_s h) \circ S_2(d_{s-1} h) \circ \cdots \circ S_2(d_1 h), \quad (19)$$

where h is the step size, $S_2(h)$ is the second-order symplectic integrator, and the composition coefficients, d_j, must satisfy the condition

$$1 = d_s + 2 \sum_{j=1}^{s-1} d_j. \quad (20)$$

For the numerical experiments in this article, we adopted (1) the 4th-order, 5-stage method of (Omelyan et al., 2002, Eq.(35)), (2) the 6th-order, 9-stage method of (Kahan and Li, 1997, `s9odr6a`), and (3) the 8th-order, 17-stage method of (Kahan and Li, 1997, `s17odr8a`). We selected these methods because they produce the least errors among the similar composition methods of the same order. The non-trivial coefficients, d_1 through d_{s-1}, of these methods are quoted in Tables 1 through 3 for the readers' convenience.

We begin with the single precision computation. Refer to Fig. 13 showing the manner of error growth of the torque-free rotation in a log-log graph. Again, we plotted the averaged results of a water molecule starting from 1000 random initial conditions while omitting the error bars in the figure.

In the case of the existing symplectic integration, unchanged is the appearance of a linear drift in the errors of the rotational energy. When the order is increased, the magnitude of the linearly-growing component increases while that of the periodic component decreases. This is because an increase in the order means an increase in the number of stages, and therefore, leads to an increase in the number of two-dimensional rotational operations.

On the other hand, in the case of the new method, an increase in the order results a decrease not only in the periodic error component but also in the secularly-growing error component, the magnitude of which grows in proportion to $\sqrt{t}$. The growth rate of 1/2 indirectly shows that the nature of the observed errors are stochastic Brouwer (1937); Henrici (1962).

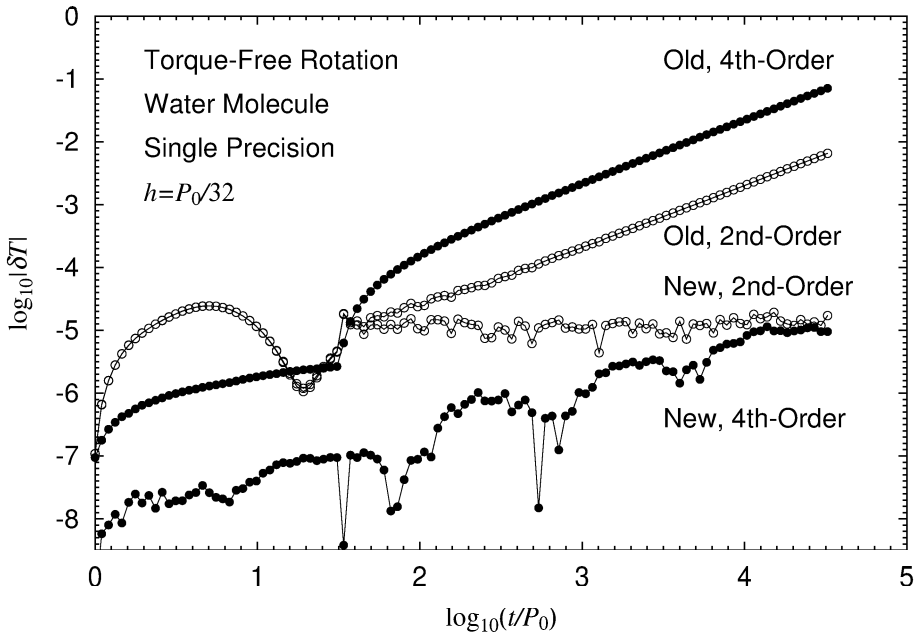

Figure 13: Effect of the order increase of the symplectic integrators. Same as Figs 1 and 2 for $h = P_0/32$ plotted in a log-log manner but added are the results of the fourth-order symplectic integrators composed from the corresponding second-order ones.

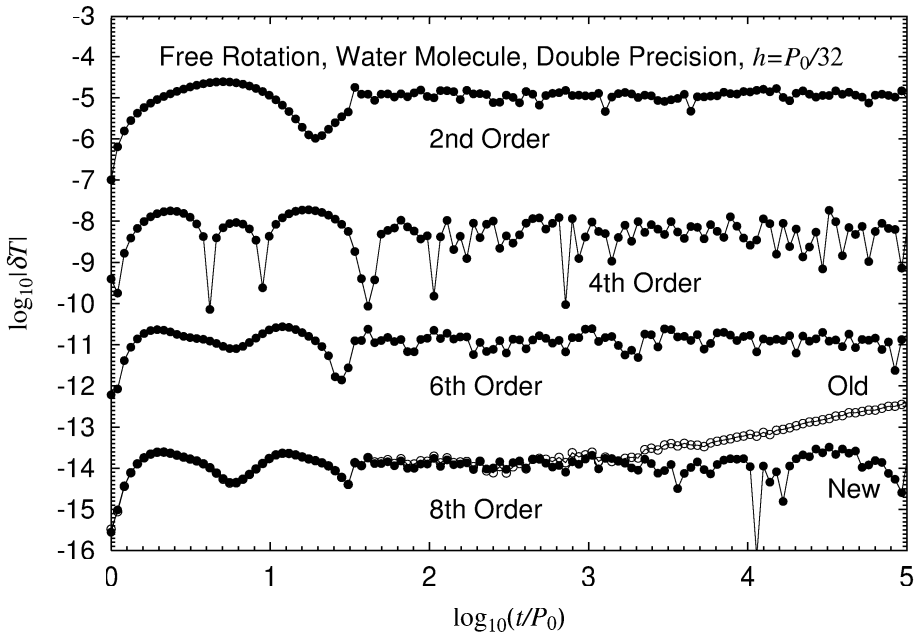

Figure 14: Applicability to the high order symplectic integrators. Same as Fig 13 but obtained by the second- through the eighth-order integrators executed in the double precision environment. The difference between the existing and the new integrators are hardly visible except for the eighth-order methods.

The difference observed in the single precision computation mostly disappears in the double precision integration. Fig. 14 illustrates the averaged energy error of the same torque-free rotation of a water molecule but computed by the second- through the eighth-order symplectic integrators in the double precision environment. Again, we omit the error bars.

In the case of the second- through the sixth-order methods, the constancy of the energy errors seems to be maintained well. Meanwhile, a small linear drift emerges after around 1000 rotation periods in the eighth-order method of the existing symplectic integration.

3.5 Long-term integration by a high order method

Comparing the results of the single and the double precision integrations presented in the previous subsections, one may think that the existing symplectic integrator is reliable if used in the double precision environment. This is not completely correct. The change of the computing precision does not resolve the problem of the accumulated round-off errors but only delays the appearance of the linearly-growing error component of the conserved quantities.

Consider a long-term integration of the torque-free rotation of a water molecule. This time, we fixed the initial condition of the body-fixed components of the angular velocity vector as

$$\frac{\omega_A}{\omega_0} = 0.5, \quad \frac{\omega_B}{\omega_0} = 0.0, \quad \frac{\omega_C}{\omega_0} = +\sqrt{1 - \left(\frac{\omega_A}{\omega_0}\right)^2 - \left(\frac{\omega_B}{\omega_0}\right)^2} \approx 0.87, \tag{21}$$

and that of the Euler parameters to specify the orientation matrix as

$$q_0 = 0.5, \quad q_1 = -0.2, \quad q_2 = -0.3, \quad q_3 = +\sqrt{1 - q_0^2 - q_1^2 - q_2^2} \approx 0.79. \tag{22}$$

The motion is as regular as seen in Fig. 15.

Fig. 16 illustrates the long-term error growth of the torque-free rotation of a water molecule obtained by the single precision symplectic integrations. We observe a similar feature as illustrated in Fig. 3, the case of the two-dimensional rotation operation. Namely, the energy errors of the existing integrators grow linearly while those of the new ones reach a plateau.

Next, we consider the rotation of a water molecule under the torque we examined in §3.2. Fig. 17 shows the feature of the rotation starting from the

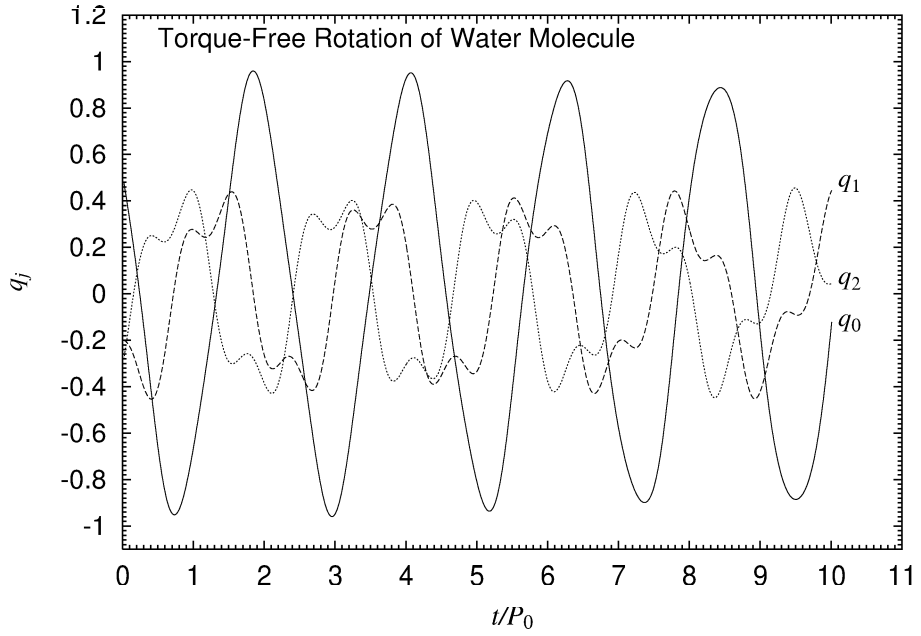

Figure 15: Behavior of a torque-free rotation of a water molecule. Depicted are the first three components of the Euler parameters, q_0, q_1, and q_2, of the torque-free rotation of a water molecule started from the initial conditions: $\omega_A/\omega_0 = 0.5$, $\omega_B/\omega_0 = 0.0$, $q_0 = 0.5$, $q_1 = -0.2$, and $q_2 = -0.3$.

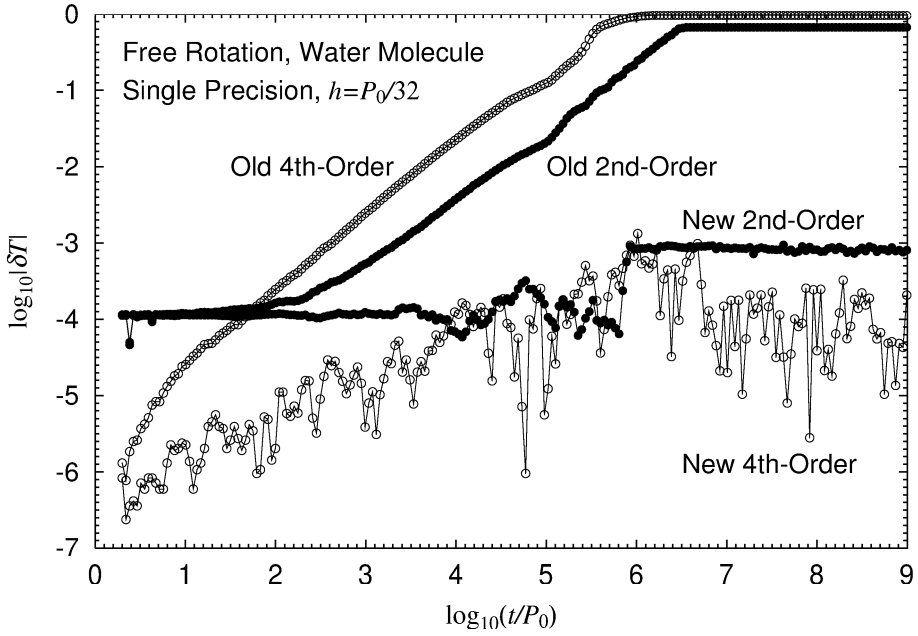

Figure 16: Long-term behavior of the low order symplectic integration. The errors of the rotational energy of a water molecule are plotted as functions of time in a log-log manner. Shown are the results obtained by the second- and the fourth-order symplectic integrators in the single precision environment for the step size $h = P_0/32$.

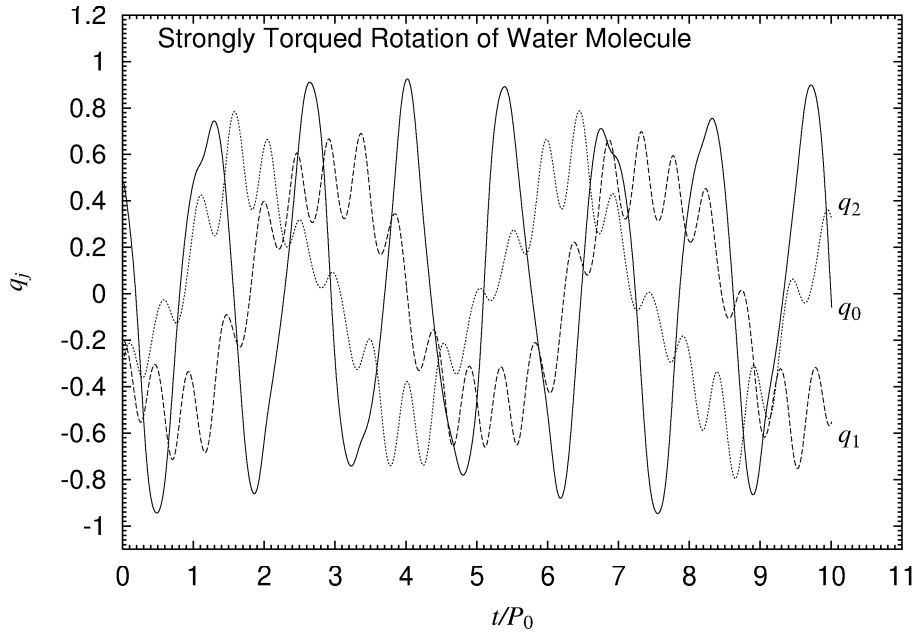

Figure 17: Behavior of the rotation of a water molecule under a strong torque. Same as Fig. 15 but for the case under the torque caused by a strong attraction toward the negative z-direction.

above initial condition for the first 10 nominal rotation periods. The rotation is fairly distorted by a strong torque as seen in Fig. 17.

Figs 18 and 19 show the long-term error growth of the total energy of this rotation obtained by the existing and new eighth-order integrators, respectively. In the case of the existing integration, linear drifts appear sooner or later. Meanwhile, the errors of the new integration seem to increase in proportion to the square root of time. This means that they are caused by the randomly produced round-off errors.

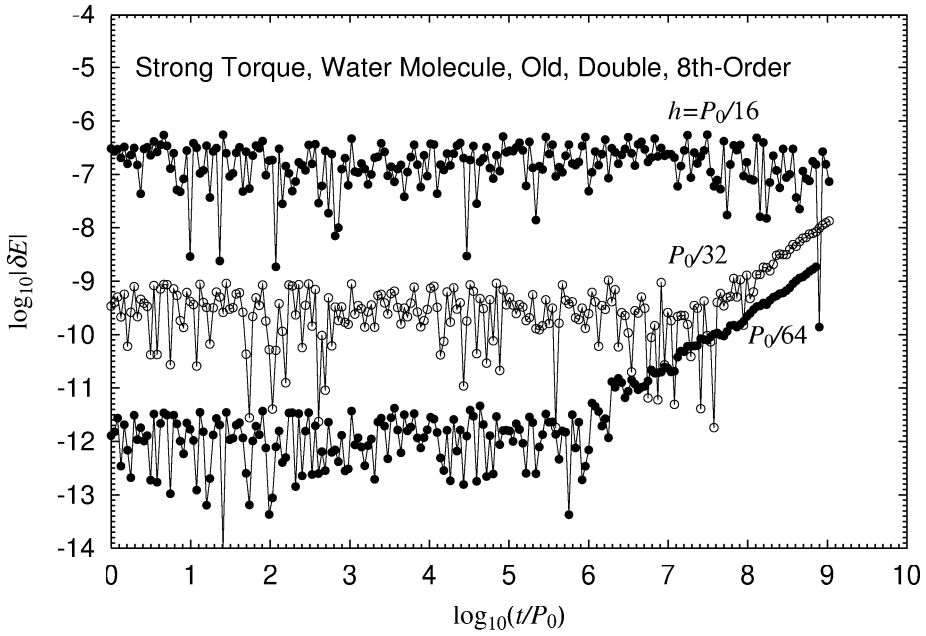

Figure 18: Long-term behavior of the existing high order symplectic integration. The errors of the total energy of a water molecule under a strong torque are plotted as functions of time in a log-log manner. The results obtained by the existing eighth-order symplectic integrator are shown for a few different step sizes.

3.6 Rotation under non-autonomous torque

Finally, we show the errors of the symplectic integrators used in simulating the rotation under a non-autonomous torque. As the rotating body, we

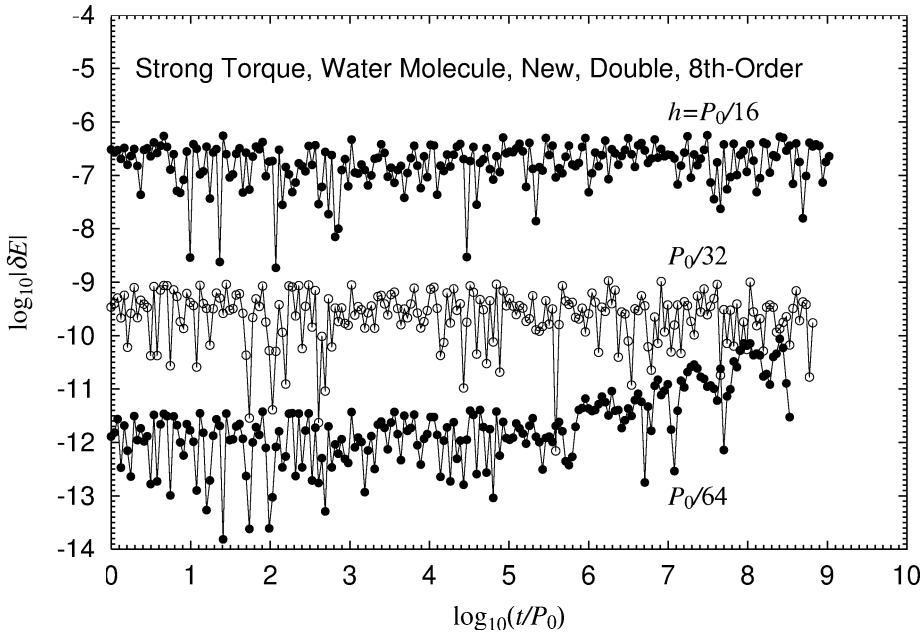

Figure 19: Long-term behavior of the new high order symplectic integration. Same as Fig. 18 but by the new eighth-order symplectic integrator.

chose the asteroid Ida. It is a lemon-shaped body with the ratios of the principal moments of inertia, $A/C = 0.23480$ and $B/C = 0.92912$. As the non-autonomous torque, we selected the gravitational tidal torque of the Sun acting on Ida while we fixed the orbit of Ida around the Sun as a pure Keplerian orbit. In Fukushima (2008a), we extensively simulated the rotation of this asteroid by high-order Adams methods in the PECE mode.

The torque expression is the same as Eq.(14) where λ and n_A through n_C are differently given as

$$\lambda \equiv \frac{GM_{\rm Sun}}{r^5}, \quad n_A \equiv \frac{\vec{r}\cdot\vec{e}_A}{r}, \quad n_B \equiv \frac{\vec{r}\cdot\vec{e}_B}{r}, \quad n_C \equiv \frac{\vec{r}\cdot\vec{e}_C}{r}. \tag{23}$$

Here $GM_{\rm Sun}$ is the heliocentric gravitational constant, $\vec{r}$ is the heliocentric position vector of the asteroid, and $r \equiv |\vec{r}|$ is its distance from the Sun.

As the orbital elements of Ida, we adopted their nominal values as (1) the semi-major axis, $a = 2.862$ AU, (2) the orbital eccentricity, $e = 0.0452$, (3) the orbital inclination, $I = 1.138$ degree, (4) the longitude of ascending node, $\Omega = 324.218$ degree, (5) the argument of perihelion, $\omega = 108.754$ degree, and (6) the mean anomaly at the perihelion passage, $M_0 = 191.869$ degree. On the other hand, we assume that the initial value of the rotational angular velocity, ω_0, is that corresponding to the observed rotation period, 0.193 day. These values imply that the relative strength of the considered torque is as small as $\approx 2.8 \times 10^{-7}$.

The considered dynamical system has no Hamiltonian. Of course, it is possible to introduce a psuedo-Hamiltonian by adding one more freedom. However, we dare not to adopt this approach and integrate the non-Hamiltonian equations of motion as if they are so. This may sound inappropriate. Nevertheless, the smallness of the perturbation in this case will allow us to reach a meaningful result as will be shown below.

Fig. 20 illustrates the relative errors of the rotation angle, ϕ, and of the norm of the orientation matrix, R. They are plotted as functions of time in a log-log manner. It is easy to obtain the errors of R since it is a mathematical constant. However, this is not the case of ϕ.

No analytical solution is available for the problem considered here. Then, we measured the errors of ϕ by comparing with the reference solution obtained by the same numerical integrator with a halved step size. Since the order of the adopted integrator is as high as 8, halving the step size makes the truncation errors of the reference solution negligibly small.

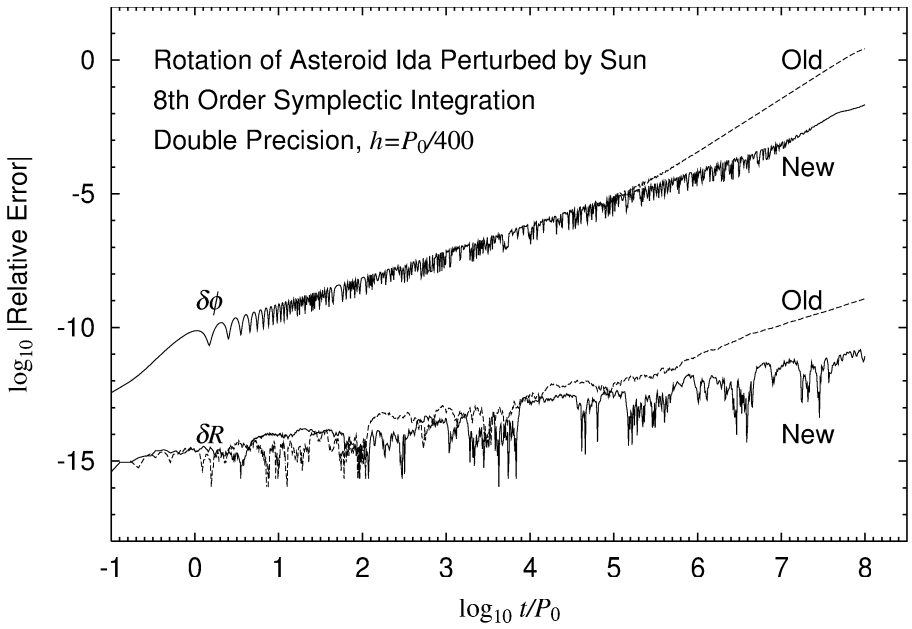

Figure 20: Long-term error growth of the rotation of the asteroid Ida under the gravitational tidal torque by the Sun. Compared are the relative errors of the rotation angle, ϕ, and the norm of the orientation matrix, R, obtained by the existing and the new eighth-order symplectic integrators.

Fig. 20 tells us that the existing symplectic integrator results a small but non-zero linear drift in $|\delta R|$, say after 10^5 rotation periods. This associates with an error component in ϕ growing quadratically with respect to time, which emerges at the same timing.

Meanwhile, the result of the new symplectic integration seems to be stochastic. Namely, the errors in R grows in proportion to $\sqrt{t}$ while those in ϕ does in proportion to $t\sqrt{t}$. This resembles the famous Brouwer's law Brouwer (1937); Henrici (1962); Hairer et al. (2008).

4 Conclusion

We observed that the accumulation of the round-off errors causes the linear drift of the conserved quantities of the rigid body rotation obtained by the existing symplectic integrators. In the single precision environment, the phenomenon is so serious that no meaningful conclusions can be extracted from the results of simulation. In the double precision computation, it becomes eminent in the long-term and high-precision integration by the high order methods.

In order to resolve this problem, we replace the two-dimensional rotation operation used in the existing symplectic integrators with its leap-frog form. The replacement costs no extra computational labor. Rather, it simplifies the rotational operation a little. On the other hand, the replacement effectively reduces the accumulation of the round-off errors. This technique works also for the high order symplectic integrators constructed by the composition method.

In conclusion, the new symplectic integrators realize a physically meaningful execution of the single precision integration of the rigid body rotation. This will open a gateway to utilize GPGPUs like the NVIDIA GeForce or the AMD/ATI Fusion in simulating a large-scale dynamical system containing the rigid body rotation.

References

Benettin, G., Cherubini, A.M., and Fassò, F., 2001 SIAM J. Sci. Comp., 23, 1189.

Bond, S.D., Leimkuhler, B.J., and Laird, B.B., 1999, J. Comp. Phys., 151, 114.

Brouwer, D., 1937, Astron. J., 46, 149.

Celledoni, E., Fassò, F., Säfström, N., and A. Zanna, A., 2007 SIAM J. Sci. Comp., 30, 2084.

Celledoni, E., and Säfström, N., 2006, J. Phys. A, 39, 5463.

Dullweber, A., Leimkuhler, B., and McLachlan, R., 1997, J. Chem. Phys. 107, 5840.

Earn, D.J. and Tremaine, S., 1992, Physica D 56, 1.

Fassò, F., 2003, J. Comput. Phys., 189, 527.

Fukushima, T., 1996, Astron. J., 112, 1298.

Fukushima, T., 2001, Astron. J., 121, 1768.

Fukushima, T., 2008a, Astron. J., 135, 2298.

Fukushima, T., 2008b, Astron. J., 136, 649

Fukushima, T., 2008c, Astron. J., 136, 1728

Fukushima, T., 2009a, Celest. Mech. Dyn. Astron., 105, 245.

Fukushima, T., 2009b, Celest. Mech. Dyn. Astron., 105, 305.

Fukushima, T., 2009c, Astron. J., 138, 210

Fukushima, T., 2010, Numer. Math., 116, 687.

Fukushima, T., 2011a, Math. Comp., 80, 1725.

Fukushima, T., 2011b, J. Comp. Appl. Math., 235, 4140.

Fukushima, T., 2011c, J. Comp. Appl. Math., 236, 1961.

Fukushima, T., 2012, Numer. Math., in printing.

Ge, Z., and Marsden, J.E., 1988, Phys. Lett. A 133, 134.

Grazier, K.R., Newman, W.I., Hyman, J.M., Sharp, P.W., and Goldstein, D.J., 2004/05, ANZIAM J., 46, C786.

Hairer, E., 2003, Numer. Math., 95, 325.

Hairer, E., Lubich, C., and Wanner, G. 2002, Geometric Numerical Integration, Springer-Verlag, Berlin

Hairer, E., McLachlan, R.I., and Razakarivony, A., 2008, BIT Numer. Math., 48, 231.

Hairer, E., Norsett, S.P., and Wanner, G. 1987, Solving Ordinary Differential Equations I, Nonstiff Problems, Springer-Verlag, Berlin

Hairer, E., and Vilmart, G., 2006, J. Phys. A: Math. Gen., 39, 13225.

Henrici, P. 1962, Discrete Variable Methods in Ordinary Differential Equations, John Wiley & Sons, Inc., New York.

Kahan, W., and Li, R.-C., 1997, Math. Comp., 66, 1089.

Karney, C.F.F., 1986, Particle Accelerators, 19, 1089.

Leimkuhler, B., and Reich, S., 2004, Simulating Hamiltonian Dynamics, Cambridge Univ. Press, Cambridge

Marsden, J. E., Pekarsky, S. and Shkoller, S., 1999, Nonlinearity, 12, 1647.

McLachlan, R.I., 1993, Phys. Rev. Lett., 71, 3043.

McLachlan, R.I., 1995, SIAM J. Sci. Comp., 16, 151.

McLachlan, R.I., and Zanna, A., 2004, Found. Comp. Math., 5, 87.

Miller, T.F., Eleftheriou, M., Pattnaik, P., Ndirango, A., Newns, D., and Martyna, G.J., 2002, J. Chem. Phys., 116, 8649.

Okumura, H., Itoh, S.G., and Okamoto Y., 2007, J. Chem. Phys., 126, 084103.

Omelyan, I.P., Mryglod, I.M., and Folk, R., 2002, Comp. Phys. Comm., 146, 188.

Ortolan, G., and Saccon, A., 2012, Int. J. Numer. Meth. Engng., 90, 390.

Petit, J.-M., 1998, Celest. Mech. Dyn. Astron., 70, 1.

Quinlan, G.D., 1994, Celest. Mech. Dyn. Astron., 58, 339.

Reich, S., 1994, Physica D 76, 375.

Sanz-Serna, J.M., 1992, Acta Numer. 1, 243.

Sanz-Sema, J.M., and Calvo, M., 1994, Numerical Hamiltonian Problems, Chapman and Hall, London.

Scovel, C., 1991, Phys. Lett. A 159, 396.

Skeel, R.D., 1999, Appl. Num. Math., 29, 3.

Touma, J., and Wisdom, J., 1994, Astron. J., 107, 1189.

van Zon, R., and Schofield, J., 2007a, J. Comput. Phys., 225, 145.

van Zon, R., and Schofield, J., 2007b, Phys. Rev. E, 75, 056701.

Vilmart, G., 2008, Physica D 76, 375.